Temporally uncorrelated photon-pair generation by dual-pump four-wave mixing

Christensen, Jesper Bjerge; McKinstrie, C. J.; Rottwitt, Karsten

Published in:
Physical Review A

Link to article, DOI:
10.1103/PhysRevA.94.013819

Publication date:
2016

Document Version
Publisher's PDF, also known as Version of record

Temporally uncorrelated photon-pair generation by dual-pump four-wave mixing

Jesper B. Christensen,[1,*] C. J. McKinstrie,[2] and K. Rottwitt[1]
[1]*Department of Photonics Engineering, Technical University of Denmark, 2800 Kongens Lyngby, Denmark*
[2]*3 Red Fox Run, Manalapan, New Jersey 07726, USA*
(Received 20 March 2016; published 11 July 2016)

We study the preparation of heralded single-photon states using dual-pump spontaneous four-wave mixing. The dual-pump configuration, which in our case employs cross-polarized pumps, allows for a gradual variation of the nonlinear interaction strength enabled by a birefringence-induced walk-off between the pump pulses. The scheme enables the preparation of highly pure heralded single-photon states, and proves to be extremely robust against the effect of nonlinear phase modulation at the required photon-pair production rates.

DOI: 10.1103/PhysRevA.94.013819

I. INTRODUCTION

Optical technologies such as quantum communication [1], quantum cryptography [2], and linear optical quantum computing [3], are key elements in contemporary science. Many of the proposals for realizing these technologies rely on processing and distributing single-photon states [4]. For this reason, a wide variety of methods have been developed with the common objective of creating a single-photon source [5]. An important subset of these methods is constituted by the nonlinear quantum-optical phenomena; spontaneous parametric down-conversion (SPDC) and spontaneous four-wave mixing (SFWM). In SPDC, which may occur in a second-order nonlinear medium, a pump photon is annihilated while two photons (conventionally referred to as the signal and idler photons) are created [6]. Similarly, SFWM can occur in a third-order nonlinear medium by creating a signal-idler photon pair at the expense of two annihilated pump photons [7]. Thus, SPDC and SFWM share the ability to create signal and idler photons that are fully correlated in their number distribution. This property can be exploited to create single photons by a technique called heralding, in which the detection of an idler (signal) photon predicts the presence of the accompanying signal (idler) photon.

Proposed schemes for realizing efficient linear optical quantum computing rely on the quantum interference between single photons [8] and require that the photons are in pure quantum-mechanical states [9,10]. However, in general, the signal and idler photons generated through SPDC or SFWM exhibit spectral and temporal correlations which compromise the purity of the heralded single-photon state [11]. This lack of purity degrades quantum interference visibility and hence decreases the obtainable efficiency in optical quantum logic gates [12].

Postprocessing of the signal-idler pair allows for purification of the heralded single-photon state. This purification can be achieved by spectrally filtering out the correlated parts of the joint signal-idler spectrum [13], or by sophisticated methods such as temporal-mode matched filtering [14] or mode-sensitive frequency conversion [15,16]. However, all of these methods share a common downside in that they result in additional photon losses and, consequently, lead to lower single-photon rates. This has provided an incentive, leading researchers to a search for a means of reducing the need for postprocess filtering and, in fact, much success has been achieved by carefully controlling the dispersion properties of the nonlinear optical waveguide [17–23]. The research has almost exclusively been focused on single-pump configurations, even though such schemes, without filtering, do not allow for entirely pure heralded single photons. This deficiency is due to unavoidable spectral-temporal correlations, which arise from the abrupt change of nonlinear interaction at the endpoints of the waveguide. On the other hand, SFWM enables dual-pump configurations [24,25], which despite their increased complexity do not necessarily suffer from the same limitation [19,26,27]. By demanding a full pump-pump walk-off inside the waveguide, a gradual variation in the nonlinear interaction can be achieved. This dual-pump configuration bears close resemblance to a scheme in which the nonlinear interaction is varied by tailoring the poling period in a quasi-phase-matched second-order nonlinear crystal [28].

In this work, we show how dual-pump SFWM can provide highly pure, heralded single-photon states. We consider a birefringent optical fiber as the waveguide, although the analysis applies to all polarization-maintaining waveguides exhibiting a significant third-order nonlinearity. The effects of self-phase modulation (SPM) and cross-phase modulation (CPM), collectively referred to as nonlinear phase modulation (NPM), are taken into account by performing a time-domain analysis of the signal-idler joint temporal amplitude (JTA). The JTA, which is related to the joint spectral amplitude by a two-dimensional Fourier transform, can be made separable in the emission times of the signal and idler photons. Full separability, however, is only achievable if the two pump pulses are allowed a full relative walk-off inside the waveguide [27]. To this end, we propose the use of type-II vectorial SFWM, where the two pumps are cross polarized, as are the generated signal and idler photons [29,30]. The group-velocity mismatch induced by birefringence facilitates the required walk-off between the pump pulses, which enables the generation of highly pure heralded single-photon states. Furthermore, we show that the introduction of NPM has only an insignificant effect on the purity of the heralded state. This is in strong contrast to recent findings for single-pump configurations [31], for which NPM was found to significantly reduce photon-state purity at the required pair-production rates.

*jesbch@fotonik.dtu.dk

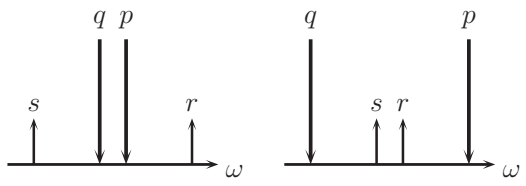

FIG. 1. Dual-pump SFWM for configurations with (left) near pumps and (right) distant pumps. Arrows pointing downward indicate photon annihilation whereas arrows pointing upward denote photon creation.

II. THEORY

This work considers photon-pair generation based on the nonlinear interaction of intense pump light in a third-order nonlinear medium. By using two pump pulses (p and q), the SFWM process enables the joint annihilation of a photon from each pump and the creation of a signal-idler photon pair (s and r). The process is restricted by frequency- and wave-number conservation

$$\begin{aligned}\Delta\omega &= \omega_p + \omega_q - \omega_r - \omega_s = 0,\\ \Delta\beta &= \beta(\omega_p) + \beta(\omega_q) - \beta(\omega_r) - \beta(\omega_s) \approx 0,\end{aligned} \tag{1}$$

where $\beta(\omega_j)$ is the propagation constant at the angular frequency ω_j, with $j \in p,q,r,s$. From these constraints, it follows that the signal-idler pair is spontaneously generated either interiorly or exteriorly with respect to the pumps, as illustrated in Fig. 1. We assume that all fields are linearly polarized along one of two principal axes of a birefringent fiber. Thus, the pumps may be either co-polarized or cross polarized, in which cases the signal-idler photon pair is also co- or cross-polarized [32].

For undepleted coherent pump pulses, the SFWM process is conveniently modelled by using coupled-mode theory. Including interpulse dispersion and assuming phase-matched fields, the governing coupled-mode equations are of the form

$$\left(\partial_z + \beta_p^{(1)}\partial_t\right)A_p = i\gamma(|A_p|^2 + \varepsilon_{pq}|A_q|^2)A_p, \tag{2a}$$

$$\left(\partial_z + \beta_q^{(1)}\partial_t\right)A_q = i\gamma(|A_q|^2 + \varepsilon_{pq}|A_p|^2)A_q, \tag{2b}$$

$$\left(\partial_z + \beta_r^{(1)}\partial_t\right)\hat{a}_r = i\gamma(\varepsilon_{rp}|A_p|^2 + \varepsilon_{rq}|A_q|^2)\hat{a}_r + i\gamma\varepsilon A_p A_q \hat{a}_s^\dagger, \tag{2c}$$

$$\left(\partial_z + \beta_s^{(1)}\partial_t\right)\hat{a}_s = i\gamma(\varepsilon_{sp}|A_p|^2 + \varepsilon_{sq}|A_q|^2)\hat{a}_s + i\gamma\varepsilon A_p A_q \hat{a}_r^\dagger, \tag{2d}$$

where $\hat{a}_{r,s}$ is the idler, signal (slowly varying) annihilation operator, $A_{p,q}$ is the complex (slowly varying) envelope of the pumps, $\beta_j^{(1)} = \partial_\omega\beta(\omega)|_{\omega=\omega_j}$ is the group slowness at the frequency of the jth field, and γ is the (common) nonlinear coupling coefficient proportional to the intensity-dependent refractive index n_2 [33]. For cross-polarized pumps, the effect of polarization enters in Eqs. (2a)–(2d) implicitly through the group slownesses $\beta_j^{(1)}$, and explicitly through the polarization-dependent coupling coefficients ε_{ij} for the CPM terms and ε for the FWM terms. For an isotropic medium such as silica, the third-order susceptibility has the tensorial property $\chi^{(3)}_{xxxx} = \chi^{(3)}_{xxyy} + \chi^{(3)}_{xyxy} + \chi^{(3)}_{xyyx}$ [34]. Therefore, the coefficients ε_{ij} and ε assume the value 2 in case of co-polarized fields and 2/3 for cross-polarized fields.

In Eq. (2), we have made the realistic assumption that the weak sidebands do not influence the classical pumps. This enables us to solve Eqs. (2a) and (2b) independently from Eqs. (2c) and (2d). By standard mathematical means the pump evolutions may be found to satisfy [35]

$$A_p(z,t) = [F_p(\xi_p)]^{1/2}\exp[i\phi_p(z,t)], \tag{3}$$

$$A_q(z,t) = [F_q(\xi_q)]^{1/2}\exp[i\phi_q(z,t)], \tag{4}$$

where the retarded times $\xi_{p,q} = t - \beta_{p,q}z$ determine the pump propagation $F_{p,q}(\xi_{p,q}) = |A_{p,q}(0,t)|^2$. Note that we have adopted the convenient notation $\beta_j \equiv \beta_j^{(1)}$. Furthermore, the pump phases $\phi_{p,q}$ are given as

$$\phi_p(z,t) = \phi_{p0}(t) + \gamma F_p(\xi_p)z + \frac{\varepsilon_{pq}\gamma}{\beta_{pq}}\int_{\xi_p}^{\xi_q} d\tau\, F_q(\tau), \tag{5}$$

$$\phi_q(z,t) = \phi_{q0}(t) + \gamma F_q(\xi_q)z + \frac{\varepsilon_{pq}\gamma}{\beta_{pq}}\int_{\xi_p}^{\xi_q} d\tau\, F_p(\tau), \tag{6}$$

with $\beta_{pq} = \beta_p - \beta_q$. Thus, from Eqs. (3)–(6), it is readily seen that the pumps evolve with unaltered shapes, while their phase profiles change due to the effects of NPM.

The signal- and idler-mode operators, which are governed by Eqs. (2c) and (2d), additionally satisfy the bosonic commutation relations

$$\begin{aligned}[\hat{a}_m(z,t),\hat{a}_n(z,t')] &= 0,\\ [\hat{a}_m(z,t),\hat{a}_n^\dagger(z,t')] &= \delta_{mn}\delta(t-t'),\end{aligned} \tag{7}$$

where $m,n \in r,s$, and δ_{mn} and $\delta(t)$ are the Kronecker and Dirac delta functions, respectively. Due to the linearity of Eqs. (2c) and (2d) in the mode operators, their solution may be written in a quantum input-output (IO) form. Denoting by $\hat{b}_{r,s}(t)$ the output mode operators at $z = l$ and output time t, and by $\hat{a}_{r,s}(t')$ the input mode operators at $z = 0$ and input time t', the IO form is

$$\hat{b}_r(t) = \int_{-\infty}^{\infty} dt'[G_{rr}(t,t')\hat{a}_r(t') + G_{rs}(t,t')\hat{a}_s^\dagger(t')], \tag{8}$$

$$\hat{b}_s(t) = \int_{-\infty}^{\infty} dt'[G_{ss}(t,t')\hat{a}_s(t') + G_{sr}(t,t')\hat{a}_r^\dagger(t')], \tag{9}$$

where G_{mn} are the Green (transfer) functions associated with the governing coupled-mode equations. These Green functions depend implicitly on the fiber length l, group slownesses β_j, and pump input profiles. As the output mode operators $\hat{b}_{r,s}$ are also subject to the commutation relations of Eq. (7), the following constraints apply to the set of Green functions:

$$\begin{aligned}[\hat{b}_r(t_r),\hat{b}_r^\dagger(t_r')] = \int_{-\infty}^{\infty} dt'[&G_{rr}(t_r,t')G_{rr}^*(t_r',t')\\ &- G_{rs}(t_r,t')G_{rs}^*(t_r',t')] = \delta(t_r - t_r'),\end{aligned} \tag{10}$$

$$\begin{aligned}[\hat{b}_r(t_r),\hat{b}_s(t_s)] = \int_{-\infty}^{\infty} dt'[&G_{rr}(t_r,t')G_{sr}(t_s,t')\\ &- G_{rs}(t_r,t')G_{ss}(t_s,t')] = 0.\end{aligned} \tag{11}$$

Since Eqs. (8) and (9) are symmetric with respect to the indices r and s, similar constraints apply upon performing the substitution $r \leftrightarrow s$ in Eqs. (10) and (11).

The Green-function formalism is convenient for describing photon statistics in optical processes such as homodyne detection, frequency conversion, and parametric amplification [36]. Moreover, it enables a simple treatment of photon-pair generation through SFWM, for which the output quantum state resulting from a two-continuous-mode vacuum input state, denoted by $|0,0\rangle$, is

$$|\psi\rangle \approx \left[1 + \int_{-\infty}^{\infty}\int_{-\infty}^{\infty} dt_s dt_r \mathcal{A}_t(t_s,t_r)\hat{a}_s^\dagger(t_s)\hat{a}_r^\dagger(t_r)\right]|0,0\rangle\,. \tag{12}$$

This (unnormalized) state contains both a vacuum and a photon-pair contribution. The temporal correlation between a signal photon at output time t_s and an idler photon at output time t_r is contained in the JTA function $\mathcal{A}_t$, which [see Appendix A] is related to the Green functions by two equivalent forms

$$\begin{aligned}\mathcal{A}_t(t_s,t_r) &= \int_{-\infty}^{\infty} dt' G_{ss}(t_s,t')G_{rs}(t_r,t') \\ &= \int_{-\infty}^{\infty} dt' G_{sr}(t_s,t')G_{rr}(t_r,t').\end{aligned} \tag{13}$$

With the goal of obtaining the JTA, we now proceed by finding the pair of Green functions G_{ss} and G_{rs}.

A. Perturbative Green functions

By definition, G_{ss} and G_{rs} are the responses obtained from an s-impulse input. In the low-gain (perturbative) regime, the FWM term in Eq. (2d) is readily neglected since the effect of the created idler on the input signal is weak. This leaves only the CPM terms in Eq. (2d), which is simplified by introducing $\hat{a}_s(z,t) = \hat{A}_s(z,t)\exp[i\phi_s(z,t)]$, with

$$\phi_s(z,t) = \gamma \sum_{j=p,q} \frac{\varepsilon_{sj}}{\beta_{sj}} \int_{t-\beta_s z}^{t-\beta_j z} d\tau F_j(\tau). \tag{14}$$

The equation for $\hat{A}_s$ is then $(\partial_z + \beta_s\partial_t)\hat{A}_s = 0$, which can be easily checked to have the Green function $H_{ss}(t,t') = \delta(t - \beta_s l - t')$. Transforming back, G_{ss} is trivially related to H_{ss} by the phase term in Eq. (14), so

$$G_{ss}(t,t') = \delta(t - \beta_s l - t')\exp[i\phi_s(l,t)]. \tag{15}$$

Thus, the effect on an input signal, in the perturbative regime, is described by a translation in time due to linear propagation and a phase change due to CPM.

Proceeding with G_{rs}, we use the time-domain collision method formulated in Refs. [26,35]. Consider an input signal-ray moving along the line from $(0,t')$ to $(l,t' + \beta_s l)$. Then the generated idler-ray exiting the waveguide at (l,t) is bound to having been created at the collision point (z_c,t_c), where

$$z_c = \frac{t' - (t - \beta_r l)}{\beta_{rs}}, \quad t_c = \frac{\beta_r t' - \beta_s(t - \beta_r l)}{\beta_{rs}}, \tag{16}$$

and we assumed that $\beta_{rs} > 0$. The effect of FWM is present only in the collision region, which is infinitesimally thin due to the impulse s input. The interaction is therefore captured by integrating Eq. (2c) across the collision region while neglecting the CPM terms. This yields the intermediate (collision) Green function

$$\begin{aligned}G_{rs}^{(c)}(t,t') = {}& i\varepsilon\bar{\gamma}(z_c,t_c)\exp[i\Phi(z_c,t_c)] \\ & \times \mathrm{H}(t' - t + \beta_r l)\mathrm{H}(t - t' - \beta_s l),\end{aligned} \tag{17}$$

where $\bar{\gamma}(z,t) = \gamma[F_p(t - \beta_p z)F_q(t - \beta_q z)]^{1/2}/\beta_{rs}$, and $\Phi(z,t) = \phi_p(z,t) + \phi_q(z,t) - \phi_s(z,t)$ is the relative phase carried over to the idler field. The Heaviside step functions $\mathrm{H}(t)$ ensure that interaction takes place only within the waveguide, i.e., $0 < z_c < l$. Outside the collision region, while propagating to the waveguide output (l,t), the generated idler solely experiences CPM from the pumps and acquires the residual phase [compare with Eq. (14)]

$$\phi_r^{(r)}(l,t) = \gamma \sum_{j=p,q} \frac{\varepsilon_{rj}}{\beta_{rj}} \int_{t_c-\beta_j z_c}^{t-\beta_j l} d\tau F_j(\tau). \tag{18}$$

It now follows from Eqs. (17) and (18) that the final form of G_{rs} is

$$\begin{aligned}G_{rs}(t,t') = {}& i\varepsilon\bar{\gamma}(z_c,t_c)\exp\left[i\Phi(z_c,t_c) + i\phi_r^{(r)}(l,t)\right] \\ & \times \mathrm{H}(t' - t + \beta_r l)\mathrm{H}(t - t' - \beta_s l).\end{aligned} \tag{19}$$

The same method enables us to find the two remaining Green functions G_{rr} and G_{sr}. Their forms are, however, nearly identical to those of G_{ss} and G_{rs}, and we therefore omit doing so here.

B. Joint temporal amplitude

Combining Eqs. (13), (15), and (19), one arrives at

$$\begin{aligned}\mathcal{A}_t(t_s,t_r) = {}& i\varepsilon\bar{\gamma}(z_c,t_c)\exp\left\{i\left[\phi_p(z_c,t_c) + \phi_q(z_c,t_c) + \phi_r^{(r)}(l,t_r)\right.\right. \\ & \left.\left. + \phi_s^{(r)}(l,t_s)\right]\right\}\mathrm{H}(t_s - t_r + \beta_{rs} l)\mathrm{H}(t_r - t_s),\end{aligned} \tag{20}$$

in which $\phi_s^{(r)}$ has the same form as Eq. (18), but with $r \to s$. In terms of the signal and idler output times t_s and t_r, the collision coordinates are given by

$$z_c = l - \frac{t_r - t_s}{\beta_{rs}}, \quad t_c = \frac{\beta_r t_s - \beta_s t_r}{\beta_{rs}}, \tag{21}$$

resulting in the modified arguments of the two Heaviside functions.

For the generation of pure-state heralded single photons, which is the main interest in this work, it is necessary for the JTA to be factorable, enabling it to be written in the uncorrelated form

$$\mathcal{A}_t(t_s,t_r) = \mathcal{A}_s(t_s)\mathcal{A}_r(t_r). \tag{22}$$

In this case, a measurement of the idler (signal) photon, brings no *additional* temporal information concerning the heralded signal (idler) photon [17]—the pair is temporally uncorrelated. In essence, this means that the temporal distributions of each of the two potential photons are determined, *a priori* and independently, by the pump-pulse durations and waveguide properties. An alternative way of seeing this is by inserting Eq. (22) into Eq. (12), after which separation of the integrals results in a product state. With this in mind, we now consider two examples for which the degree of factorability differs greatly.

Examples

For the examination of the JTA, and for the remaining part of the paper, we model the input pumps as unchirped Gaussian profiles

$$A_p(t) = \left(\frac{E_p}{\pi^{1/2}\tau_p}\right)^{1/2} \exp\left[\frac{-(t+\beta_p z_0)^2}{2\tau_p^2}\right], \qquad (23)$$

where E_p is the pulse energy, and τ_p is the pulse width. The amplitude profile for pump q is similar. The length variable z_0 indicates the distance-coordinate in the waveguide, where the pumps are maximally overlapped. We consider only the symmetric case $z_0 = l/2$, for which the overlap between the pulsed pumps is largest at the waveguide midpoint.

Neglecting the contribution from NPM, Fig. 2 illustrates the JTA function in two vastly different cases. The white dashed lines indicate the waveguide endpoints (bottom-beginning and top-end), which are mathematically described by the Heaviside functions. In Fig. 2(a), we show the standard case

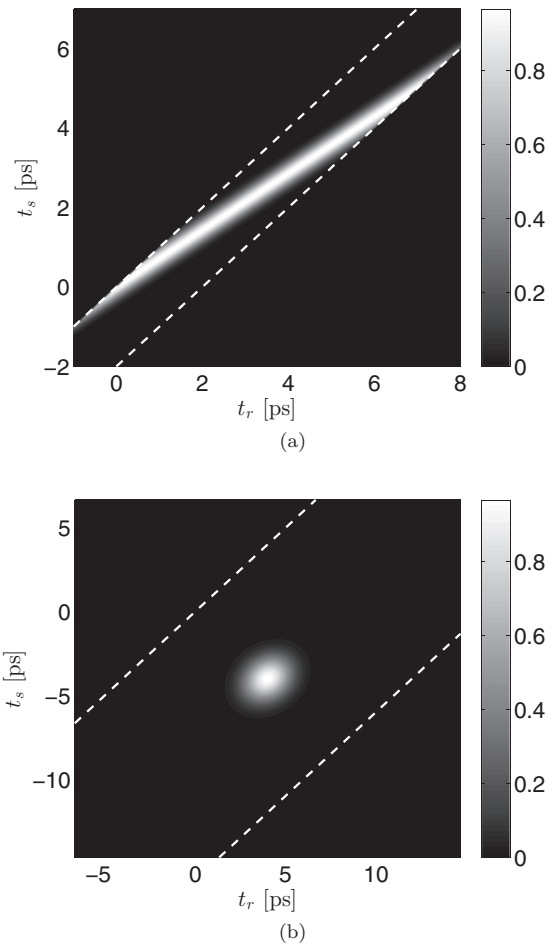

FIG. 2. Absolute value of the JTA for two different cases of dispersion, but identical pump durations $\tau_p = \tau_q = \tau = 1$ ps, and fiber length $l = 10$ m. In panel (a) $\beta_{pq} = 0$ ps/m, $\beta_{sq} = 0.5$ ps/m, and $\beta_{rp} = 0.7$ ps/m, while in panel (b) $\beta_{pq} = 2$ ps/m, $\beta_{sq} = 0.2$ ps/m, and $\beta_{rp} = -0.2$ ps/m. The latter configuration illustrates how pump-pump walk-off enables a gradually varying interaction which is strongest at the fiber midpoint.

with $\beta_p \approx \beta_q < \beta_s \approx \beta_r$, typically obtained for co-polarized pumps placed in close vicinity of a waveguide zero-dispersion frequency. Since the pumps are propagating at similar speeds, this situation is comparable to what may be obtained using single-pump configurations. The JTA, in this case, exhibits large temporal correlation in the signal-idler photon pair. This is typical for single-pump configurations although the degree of correlation may be greatly reduced by virtue of dispersion engineering. Especially two cases have been exhaustively studied and demonstrated, for which the JTA is oriented either horizontally (vertically) [18] or at an angle of -45° [17]. However, both of these configurations exhibit strong abrupt changes in nonlinear interaction at the waveguide endpoints resulting in the well-known sinc-like behavior of the joint spectral amplitude [13,21]. The JTAs of these configurations have recently been carefully analyzed in Ref. [31], and are therefore omitted here. To circumvent the issue related to the sinc-like behavior, one may instead exploit the extra degree of freedom enabled by a dual-pump configuration as shown in Fig. 2(b). In this situation, the nonlinear interaction is, due to pump-pump walk-off, absent near the waveguide endpoints (see Appendix B). Although the shown JTA does exhibit a small degree of correlation, it is possible to make it factorable. In particular, correlation is absent if the JTA contours are oriented either vertically, horizontally, or have common eccentricity of 0 (are circular). This is the subject of the following section.

C. Purity criterion

The temporal purity of a heralded photon can be extracted from the biphoton part of the SFWM-produced quantum state

$$|\psi_1\rangle = \iint dt_s dt_r \mathcal{A}_t(t_s,t_r)\hat{a}_s^\dagger(t_s)\hat{a}_r^\dagger(t_r)\,|0,0\rangle\,, \qquad (24)$$

by performing either of the traces $\mathcal{P} = \mathrm{Tr}(\pi_s^2) = \mathrm{Tr}(\pi_r^2)$, where $\pi_{s,r} = \mathrm{Tr}_{r,s}(|\psi\rangle\langle\psi|)$ are the density operators associated with the signal and idler subsystem, respectively. (See Appendix C for a detailed analysis of the heralding process.) Irrespective of the subsystems considered, the purity may be formulated as the quadruple integral [27]

$$\mathcal{P} = \frac{1}{R^2}\iiiint dt_s dt_r dt_s' dt_r' \mathcal{A}_t(t_s,t_r) \times \mathcal{A}_t^*(t_s',t_r)\mathcal{A}_t^*(t_s,t_r')\mathcal{A}_t(t_s',t_r'), \qquad (25)$$

where R is the photon-pair production rate (probability of pair generation per pair of pump pulses), which is included to normalize the heralded single-photon state

$$R = \iint dt_s dt_r |\mathcal{A}_t(t_s,t_r)|^2. \qquad (26)$$

For reasons made apparent in the preceding section, we are particularly interested in cases where a full pump-pump collision is allowed in the waveguide. It is therefore intriguing to neglect the Heaviside functions in the JTA, enabling an analytical evaluation of Eq. (25):

$$\mathcal{P}_f = \frac{\sigma_{p,q}|\beta_{rp}\beta_{sq} - \beta_{rq}\beta_{sp}|}{\sqrt{\left(\beta_{rp}^2 + \beta_{rq}^2\sigma_{p,q}^2\right)\left(\beta_{sp}^2 + \beta_{sq}^2\sigma_{p,q}^2\right)}}, \qquad (27)$$

in which we have defined the fractional pump width as $\sigma_{p,q} = \tau_p/\tau_q$. Under the same assumptions, and using the fact that $\beta_{rp}\beta_{sq} - \beta_{rq}\beta_{sp} = \beta_{rs}\beta_{pq}$, one finds the full pump-pump collision generation rate given as

$$R_f = \frac{\varepsilon^2\gamma^2 E_p E_q}{|\beta_{rs}\beta_{pq}|}. \tag{28}$$

Note that Eq. (27) is only strictly valid without the effects of NPM, and should therefore be considered mostly as a guideline at low and moderate pair-production rates ($R < 0.1$), for which occurrences of multiphoton pair states can readily be neglected. Equation (28) offers a reference for the generation rate R, and it is noteworthy that the full collision pair-production rate R_f depends on the pulse energies and is independent of the waveguide length. Instead, the important length scale is the effective interaction distance, which is determined by the interpulse walk-off between the two pumps [27]. Moreover, Eq. (27) leads to an important criterion for unit purity, stating that the relative group slownesses and pump-pulse widths should satisfy the relationship

$$\beta_{rp}\beta_{sp} = -\sigma_{p,q}^2\beta_{rq}\beta_{sq}. \tag{29}$$

This result, which may also be obtained by requiring $\bar{\gamma}(z_c,t_c)$ to be separable [see Eq. (20)], is in agreement with the findings of Ref. [27], in which a similar analysis was performed in the spectral domain. We emphasize that the criterion in Eq. (29), should not be satisfied by letting $\beta_{pq} = 0$ or $\beta_{rs} = 0$, because both of these situations contradict the assumption of neglecting the Heaviside functions. Instead, the criterion can be satisfied *symmetrically* by pairwise pump-signal group-velocity matching, i.e., $\beta_p = \beta_r$ and $\beta_q = \beta_s$, or *asymmetrically* by requiring either $\beta_p > \beta_r > \beta_q > \beta_s$ or $\beta_r > \beta_p > \beta_s > \beta_q$, while at the same time tuning the fractional pump width $\sigma_{p,q}$. It is not in general straightforward to realize waveguide dispersions, which simultaneously satisfy the phase-matching condition and the purity criterion in Eq. (29), but a likely solution incorporates linearly cross-polarized pumps (see Sec. IV). With such a configuration, an extra degree of freedom is available for controlling the group slownesses of the participating fields. In particular, it becomes possible to introduce group-velocity mismatches at like frequencies due to fiber birefringence. Thus, adapting to a situation where the signal s and pump p are co-polarized and cross-polarized compared to the idler r and pump q, results in $\varepsilon_{rp} = \varepsilon_{sq} = \varepsilon_{pq} = \varepsilon = 2/3$ and $\varepsilon_{rq} = \varepsilon_{sp} = 2$ [33], which we use in the remaining part of this paper.

III. NUMERICAL STUDIES

A. The Schmidt decomposition

The four Green functions have the Schmidt decompositions [37,38]

$$G_{rr}(t,t') = \sum_{j=1}^{\infty} v_{rj}(t)\mu_j u_{rj}^*(t'), \tag{30a}$$

$$G_{rs}(t,t') = \sum_{j=1}^{\infty} v_{rj}(t)\nu_j u_{sj}(t'), \tag{30b}$$

$$G_{sr}(t,t') = \sum_{j=1}^{\infty} v_{sj}(t)\nu_j u_{rj}(t'), \tag{30c}$$

$$G_{ss}(t,t') = \sum_{j=1}^{\infty} v_{sj}(t)\mu_j u_{sj}^*(t'), \tag{30d}$$

for which each pair of the (real) Schmidt coefficients μ_j and ν_j obey the auxiliary equation $\mu_j^2 - \nu_j^2 = 1$ [38], and the output v_{kj} and input u_{kj} Schmidt modes for $k \in r,s$ constitute four orthonormal sets. These decomposed forms of the Green functions allow us to gain additional insight regarding the JTA. Inserting the Schmidt decompositions of Eq. (30) into Eq. (13), the JTA may be formulated by its own Schmidt decomposition

$$\mathcal{A}_t(t_s,t_r) = \sum_{j=1}^{\infty} \lambda_j v_{sj}(t_s)v_{rj}(t_r), \tag{31}$$

in which $\lambda_j = \mu_j\nu_j$ are the resulting Schmidt coefficients. In the regime of low pair-generation rate, $\nu_j \ll 1$, $\mu_j \approx 1$, and hence $\lambda_j \approx \nu_j$. The basis functions of the JTA are seen to be the output Schmidt modes v_{rj} and v_{sj} of the Green functions—in agreement with intuition. This also explains the reason for the pairing of G_{rr} with G_{sr} and G_{ss} with G_{rs} in Eq. (13). It is noteworthy that the separability of G_{rs} and G_{sr} is both a necessary and sufficient condition for achieving a separable JTA. This implies that one only needs to determine G_{rs} or G_{sr} to establish the separability of the JTA. The Green functions may also be found numerically by employing the method from Refs. [39,40].

It now follows from inserting Eq. (31) into Eq. (26) that the pair-generation rate is obtained simply as

$$R = \sum_{j=1}^{\infty} \lambda_j^2. \tag{32}$$

Thus, the coefficients λ_j^2 should be interpreted as the generation probability (per set of pump pulses) of a signal-idler photon pair with respective temporal wave-packet profiles v_{sj} and v_{rj}. Similarly, by inserting Eq. (31) into Eq. (27), the photon purity is expressed as

$$\mathcal{P} = \frac{1}{R^2}\sum_{j=1}^{\infty} \lambda_j^4 \leqslant 1, \tag{33}$$

for which the ideal case of unity corresponds to no temporal entanglement between the signal and idler photons. This situation is obtained, only if the JTA has a Schmidt rank of unity (separable) so that it may be expressed as the product between a single set of temporal wave-packet modes, i.e., $\mathcal{A}_t(t_s,t_r) = \lambda_1 v_{s1}(t_s)v_{r1}(t_r)$.

B. Numerical results

By employing numerical tools for calculating the singular value decomposition of the Green functions, as described in Sec. III A, it is straightforward to obtain the photon purity and the photon-pair production rate for any given JTA. In the following, we do so for various fiber characteristics while directing much of our attention to the effect of NPM. Because Eqs. (27) and (29) were derived without the effect of NPM, we

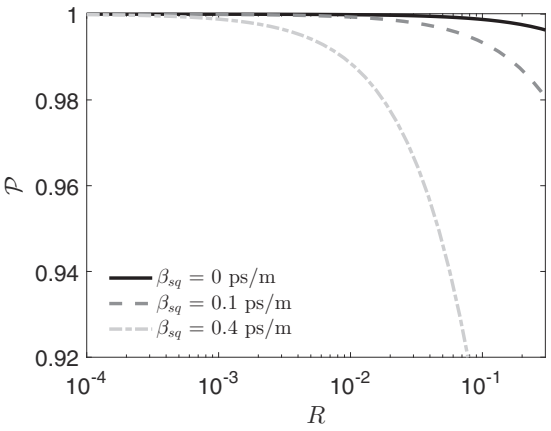

FIG. 3. Temporal purity $\mathcal{P}$ plotted versus the pair-production rate R for $\beta_{pq} = 2$ ps/m, fiber length $l = 10$ m, and common pump duration $\tau = 1$ ps. At moderate and high pair-production rates, the symmetrically group-velocity-matched case $\beta_{sq} = \beta_{rp} = 0$ ps/m is least affected by the effects of NPM.

only expect these expressions to be valid in the regime of very low pair-production rates. However, the analytic results allow a direct investigation of how NPM affects the single-photon purity in various cases.

Figure 3 shows how the purity $\mathcal{P}$ is degraded by NPM for increasing pair-production rates R for $\beta_{pq} = 2$ ps/m, a fiber length of $l = 10$ m, and identical pump durations of $\tau_p = \tau_q = 1$ ps. The figure shows both the symmetrically-group-velocity-matched case $\beta_{sq} = 0$ ps/m, and two cases with different degrees of asymmetric group-velocity matching $\beta_{sq} = 0.1$ ps/m and $\beta_{sq} = 0.4$ ps/m. In all cases, the value of β_r is chosen to satisfy the purity criterion of Eq. (29), as is apparent from the fact that all three cases converge to a purity of unity at small pair-production rates. Moreover, this means that the chosen parameters resulted in a full symmetric pump-pump collision in the fiber. It is evident that the effect of NPM has an enhanced impact on the purity as the value of β_{sq} increases, showing that the symmetrically-group-velocity-matched case is least affected by NPM. In fact, the case $\beta_{sq} = 0$ ps/m shows almost ideal behavior with purities $\mathcal{P} > 0.999$ for pair-production rates as high as $R = 0.08$. However, both of the considered asymmetrically group-velocity matched cases also exhibit large purities ($\mathcal{P} > 0.98$) for pair-production rates $R < 0.02$.

Figure 4 shows both the amplitude and the phase of a symmetrically- and an asymmetrically-group-velocity-matched JTA. In both cases the interaction strength was chosen to give a pair-production rate of $R = 0.02$. Furthermore, a full pump-pump collision was achieved by using a fiber length of $l = 5$ m, pump durations of $\tau_p = \tau_q = 1$ ps, and a difference in group slowness between the pumps of $\beta_{pq} = 2$ ps/m. For the symmetrically-group-velocity-matched case, which is shown in Figs. 4(a) and 4(c), the pumps and sidebands are pairwise matched in group slowness, so that $\beta_{sq} = \beta_{rp} = 0$ ps/m. In this case, the JTA amplitude is simply the product of two independent Gaussian distributions of different mean values but identical widths. The two mean values correspond to the average output times of the signal and idler photons given by $\beta_r l/2$ and $\beta_s l/2$, respectively. Thus the idler photon is on average retarded by a factor $\Delta_{rs} = \beta_{rs} l/2 = 5$ ps with respect to the signal photon, as expected for a symmetric collision between the pumps. Note that the output times are relative to an average frame of reference for which $\beta_p = -\beta_q$ and should not be interpreted as absolute times. The JTA phase shows how NPM from the pulsed pumps results in bell-like chirps in the signal and idler output times. Furthermore, the JTA phase displays a large degree of symmetry, which is why the symmetrically-group-velocity-matched case is only slightly affected by the effects of NPM. However, upon close inspection, temporal correlation is found along a line at -45° through the interaction region. This correlation arises due to the fact that a photon pair created at the beginning of the pump-pump overlap (fourth quadrant with respect to the interaction region), pairwise experience CPM while colliding with the group-velocity mismatched pump (s with p and r with q). In contrast, a photon pair generated at the end of the pump-pump overlap is not subject to any significant CPM from the group-velocity mismatched pump (second quadrant with respect to the interaction region). Notably, this phase asymmetry increases for higher pair-production rates and thereby limits the purity, as observed in Fig. 3. In Figs. 4(b) and 4(d), the asymmetrically-group-velocity-matched case is shown for $\beta_{sq} = 0.25$ ps/m, while β_r is chosen to satisfy the criterion in Eq. (29). The JTA amplitude remains a separable function of the output times, although the temporal wave-packet mode of an idler photon is now broader than that of a signal photon. However, with asymmetric group-velocity matching, the branches in the JTA phase are seen to depart from being horizontal and vertical, introducing enhanced (phase) correlation in the signal-idler biphoton temporal amplitude.

IV. SIMULTANEOUS PHASE- AND GROUP-VELOCITY MATCHING

Until this point, we have postponed the issue of simultaneously achieving phase-matching as described by Eq. (1) and group-velocity matching as formulated in Eq. (29). Potentially, these conditions can be concurrently met by placing two co-polarized pumps far apart in frequency to enable a full pump-pump walk-off [27]. In this case, high-purity single-photon states may be obtained by engineering the phase-matching condition such that the signal-idler pair is generated at the orthogonal polarization in close spectral vicinity to each their pump. In search for a more versatile alternative, we here show that both conditions are readily satisfied by instead using the configuration of cross-polarized pumps. As shown in Fig. 5, this configuration comes in two different versions; frequency-degenerate pumps (left) and frequency-nondegenerate pumps (right). Both versions have their own distinct advantage: whereas the former is simple and easily realized using a single laser source, the latter contains an extra degree of freedom and so allows for more tunability.

The phase-matching condition can be explored by expanding the propagation constant $\beta(\omega)$ to second order around the average pump center-frequency $\omega_a = (\omega_p + \omega_q)/2$. By adopting the notation $\Omega_i = \omega_i - \omega_a$ and using the fact that $\Omega_q = -\Omega_p$ and $\Omega_s = -\Omega_r$, the phase-matching condition

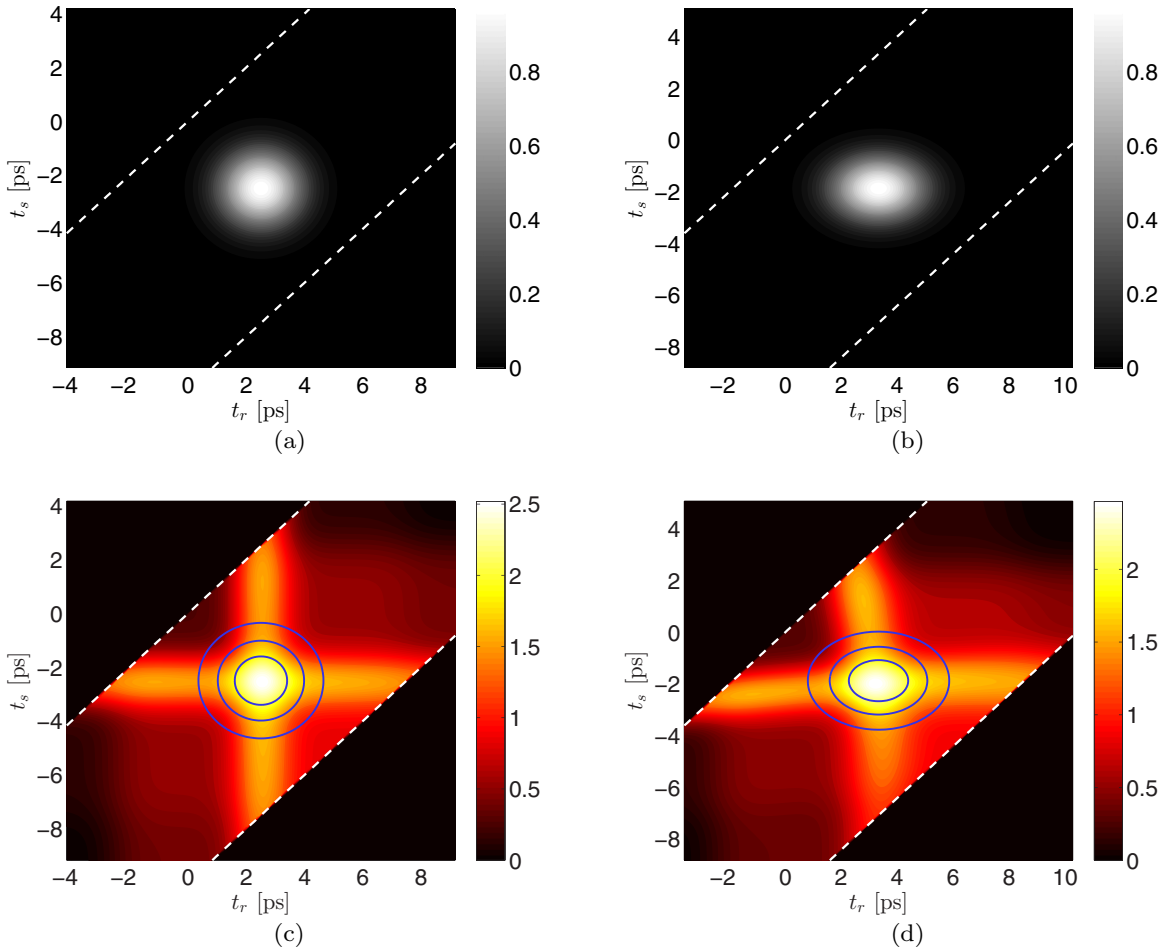

FIG. 4. JTA amplitude (top) and phase (bottom) for symmetric group-velocity matching (left) and asymmetric group-velocity matching (right). In both cases, we used a fiber length of $l = 5$ m, a common pump duration of $\tau = 1$ ps, and a difference in group slowness between the pumps of $\beta_{pq} = 2$ ps/m. In the asymmetrically-group-velocity-matched case, the difference in group slowness between pump q and the signal s was $\beta_{sq} = 0.25$ ps/m, resulting in a noticeable skewness in the phase profile of the JTA. The blue solid lines in the JTA phases indicate contour lines of the corresponding JTA amplitudes, while the white dashed lines, as previously, indicate the bounding region of the Heaviside functions.

becomes

$$\Delta\beta = \Delta\beta^{(1)}(\Omega_p + \Omega_r) + \beta^{(2)}\left(\Omega_p^2 - \Omega_r^2\right), \tag{34}$$

where we defined $\Delta\beta^{(1)} = \beta_x^{(1)} - \beta_y^{(1)}$ with the subscripts denoting axis of linear polarization. Additionally, we made the reasonable assumption that $\beta^{(2)}$ is independent of polarization [33]. It directly follows from Eq. (34) that $\Delta\beta = 0$ requires the frequencies to obey

$$\Delta\beta^{(1)} = -\beta^{(2)}(\Omega_p - \Omega_r), \tag{35}$$

or equivalently

$$\Delta\beta^{(1)} = \beta^{(2)}(\Omega_q - \Omega_s). \tag{36}$$

Notably, since the sign of $\Delta\beta^{(1)}$ can be altered simply by exchanging the pump input polarizations with respect to the waveguide slow and fast axes, the phase-matching condition can be satisfied for both positive and negative values of $\beta^{(2)}$. Moreover, Eqs. (35) and (36) express the fact that the proposed setup is versatile in terms of tunability: the frequency of the idler depends only on the frequency of the oppositely polarized pump p (and similarly for the signal and pump q). Therefore, by shifting the frequency of pump p, it is possible to tune the idler frequency independently of the signal frequency, and *vice versa*.

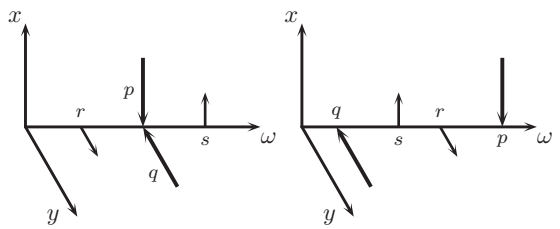

FIG. 5. Dual-pump cross-polarized SFWM with (left) frequency-degenerate pumps and (right) frequency-nondegenerate pumps. Both configurations produce cross-polarized signal-idler photon pairs.

To explore the prospects of achieving the required group-slowness matching as described by Eq. (29), Fig. 6 shows an example of the group-slowness curves for (a) frequency-degenerate pumps and (b) frequency-nondegenerate pumps.

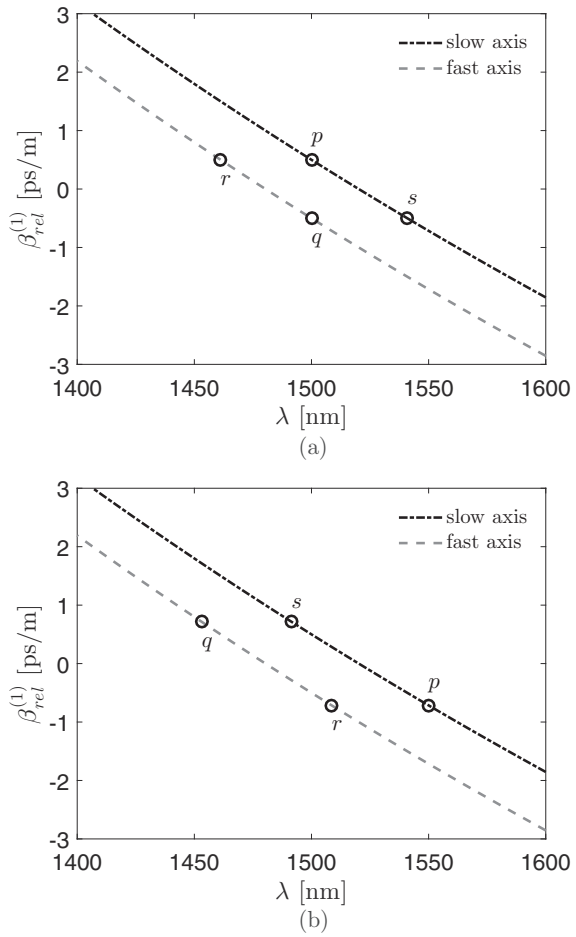

FIG. 6. Relative group-slowness curves with $\Delta\beta^{(1)} = 1$ ps/m and $\beta^{(2)} = 0.03$ ps^2/m for (a) degenerate pumps and (b) distant pumps with interiorly placed signal and idler waves.

The wavelengths of the pumps and the phase-matched signal and idler, are marked on the curves to enable a comparison of the relative group slownesses. It appears that, irrespective of the configuration used, the idler (signal) is generated at a wavelength so that it copropagates with the orthogonally polarized pump p (q). This is clarified by evaluating the relative slowness β_{rp} (β_{sq}):

$$\beta_{rp} = -\Delta\beta^{(1)} - \beta^{(2)}(\Omega_p - \Omega_r) = -\beta_{sq}. \tag{37}$$

At phase-matched frequencies, which obey Eqs. (35) and (36), the effect of Eq. (37) is that $\beta_{rp} = \beta_{sq} = 0$. Thus, in the configuration of cross-polarized pumps considered here, the signal-idler pair is pairwise group-velocity matched to the pumps; the optimal situation with respect to purity of a heralded single-photon state.

V. CONCLUSION

In this paper, we considered a scheme for generating photon pairs using dual-pump spontaneous four-wave mixing in a third-order nonlinear medium. This configuration enables a controlled evolution of the nonlinear interaction inside the waveguide due to pump-pump walk-off. In particular, the case in which the pumps walk fully through each other inside the nonlinear medium holds great promise for preparing highly pure single-photon states. To show this, we derived a criterion depending only on the group slownesses and pump durations, which, when satisfied, renders the signal- and idler photons temporally uncorrelated in the regime of low generation rates. At high generation rates, pump-induced nonlinear phase modulation introduces temporal phase correlations within the signal-idler pair, resulting in a photon of degraded purity. However, the observed impact was much weaker than that of Ref. [31], in which a similar analysis was performed for single-pump configurations. In particular, for the case of symmetric group-velocity matching, in which the signal-idler photons each copropagate with one of the pump pulses, the effects of nonlinear phase modulation were insignificant for pair-production rates (probabilities) as high as 0.1. Finally, we showed how this symmetrically-group-velocity-matched case is readily realized by cross-polarized pumps in a birefringent waveguide.

ACKNOWLEDGMENT

J.B.C. was supported by the DFF Sapere Aude Adv. Grant NANO-SPECs.

APPENDIX A: UNITING THE HEISENBERG AND SCHRÖDINGER REPRESENTATIONS

This paper contains formulations originating from both the Heisenberg picture (HP) and the Schrödinger picture (SP). Whereas the IO relations, describing the quantum operator evolution, derive from the HP, the JTA, used to describe the quantum-state evolution, clearly originates from the SP. In the following, we unite these descriptions by deriving a relation between the Green functions and the JTA. The same method has been used in a study of photon-pair generation by single-pump SFWM [41].

A necessary result stems from the fact that the sideband evolution is unitary. This property entails that the IO relations given by Eqs. (8) and (9) are accompanied by a similar set of output-input relations. The corresponding (backward) transfer functions are related to the (forward) transfer Green functions in a way so the output-input relations read [36]

$$\hat{a}_r(0,t') = \int_{-\infty}^{\infty} dt[G_{rr}^*(t,t')\hat{b}_r(l,t) - G_{sr}(t,t')\hat{b}_s^\dagger(l,t)], \tag{A1}$$

$$\hat{a}_s(0,t') = \int_{-\infty}^{\infty} dt[G_{ss}^*(t,t')\hat{b}_s(l,t) - G_{rs}(t,t')\hat{b}_r^\dagger(l,t)]. \tag{A2}$$

Note especially that integration is now performed with respect to the first argument of the Green functions.

Now suppose that an input state is given by the two-mode vacuum, $|\psi(z=0)\rangle = |0,0\rangle$, so that

$$\hat{a}_r(0,t')\,|\psi(0)\rangle = 0, \quad \hat{a}_s(0,t')\,|\psi(0)\rangle = 0. \tag{A3}$$

By inserting Eq. (A1) into the first of Eq. (A3), one finds

$$\int_{-\infty}^{\infty} dt[G_{rr}^*(t,t')\hat{b}_r(l,t) - G_{sr}(t,t')\hat{b}_s^\dagger(l,t)]\,|\psi(0)\rangle = 0, \tag{A4}$$

which involves the input state vector $|\psi(0)\rangle$ and the output mode operators $\hat{b}_j(l,t)$ and is therefore clearly written in

the HP. Converting the mode operators to the SP requires introduction of the unitary (squeezing) operator $\hat{U}(l)$, which evolves the state vector according to $\hat{U}(l)\,|\psi(0)\rangle = |\psi(l)\rangle$. Operating from the left with $\hat{U}(l)$ on Eq. (A4) results in

$$\hat{U}(l)\int_{-\infty}^{\infty} dt[G^*_{rr}(t,t')\hat{b}_r(t) - G_{sr}(t,t')\hat{b}^\dagger_s(t)]\,|\psi(0)\rangle = \int_{-\infty}^{\infty} dt[G^*_{rr}(t,t')\hat{a}_r(t) - G_{sr}(t,t')\hat{a}^\dagger_s(t)]\,|\psi(l)\rangle = 0, \tag{A5}$$

where we have made use of the operator transformation $\hat{a}_j = U(l)\hat{b}_j U^\dagger(l)$ [42] and inserted the identity $U^\dagger(l)U(l)$ before the state vector. Note also that we have omitted the spatial dependence of the mode operators because it is obvious from the context ($\hat{b}_j$ is an evolved operator in the HP and $\hat{a}_j$ is the static operator in the SP).

Following a perturbative approach to first order, we now solve Eq. (A5) approximately for the state vector $|\psi(l)\rangle$. This comprises that we introduce the expansion

$$|\psi(l)\rangle \approx |\psi_0\rangle + |\psi_1\rangle\,, \tag{A6}$$

where $\langle\psi_0|\psi_0\rangle \gg \langle\psi_1|\psi_1\rangle$, and moreover assume that the second term in Eq. (A5) (involving G_{sr}) is a first-order term while the first term (involving G_{rr}) is a zeroth-order term. This immediately allows a partition of Eq. (A5) into its zero-order components

$$\int_{-\infty}^{\infty} dt\,G^*_{rr}(t,t')\hat{a}_r(t)\,|\psi_0\rangle = 0, \tag{A7}$$

and its first-order components

$$\int_{-\infty}^{\infty} dt\,G^*_{rr}(t,t')\hat{a}_r(t)\,|\psi_1\rangle = \int_{-\infty}^{\infty} dt\,G_{sr}(t,t')\hat{a}^\dagger_s(t)\,|\psi_0\rangle\,. \tag{A8}$$

Equation (A7), together with the corresponding equation for the signal, is satisfied by the two-mode vacuum state. Thus, the zeroth-order equation, unsurprisingly, has the solution $|\psi_0\rangle = |0,0\rangle$. In order to solve the first-order equation described by Eq. (A8), consider

$$\int_{-\infty}^{\infty} dt\,G^*_{rr}(t,t')\hat{a}_r(t)\int_{-\infty}^{\infty}\int_{-\infty}^{\infty}\int_{-\infty}^{\infty} dt_r d\bar{t}_r dt_s \times G_{rr}(t_r,\bar{t}_r)G_{sr}(t_s,\bar{t}_r)\hat{a}^\dagger_r(t_r)\hat{a}^\dagger_s(t_s)\,|0,0\rangle\,. \tag{A9}$$

To simplify Eq. (A9), one can use the commutation relation for $\hat{a}_r$ and $\hat{a}^\dagger_r$ given in Eq. (7) in addition to the constraints it forces upon the Green functions through Eq. (A1). This constraint links the first arguments of G^*_{rr} and G_{rr} according to

$$\int_{-\infty}^{\infty} dt_r\,G^*_{rr}(t_r,t')G_{rr}(t_r,\bar{t}_r) \approx \delta(t'-\bar{t}_r), \tag{A10}$$

which is similar to Eq. (10), but with the integration performed with respect to the first arguments rather than the second. Equation (A9) now reduces to

$$\int_{-\infty}^{\infty} dt_s\,G_{sr}(t_s,t')\hat{a}^\dagger_s(t_s)\,|0,0\rangle\,, \tag{A11}$$

which is clearly identical to the right-hand-side of Eq. (A8). Thus, from Eqs. (A9)–(A11) it is evident that the first-order perturbative state vector $|\psi_1\rangle$ is

$$|\psi_1\rangle = \int_{-\infty}^{\infty}\int_{-\infty}^{\infty} dt_s dt_r \mathcal{A}_t(t_s,t_r)\hat{a}^\dagger_s(t_s)\hat{a}^\dagger_r(t_r)\,|0,0\rangle\,, \tag{A12}$$

where the integral kernel (joint temporal amplitude) has the form

$$\mathcal{A}_t(t_s,t_r) = \int_{-\infty}^{\infty} d\bar{t}\,G_{sr}(t_s,\bar{t})G_{rr}(t_r,\bar{t}). \tag{A13}$$

Note that using the signal (second) part of Eq. (A3) results in the alternative expression

$$\mathcal{A}_t(t_s,t_r) = \int_{-\infty}^{\infty} d\bar{t}\,G_{ss}(t_s,\bar{t})G_{rs}(t_r,\bar{t}), \tag{A14}$$

in conformity with the constraints set by the commutation relation in Eq. (11).

APPENDIX B: ANALYTIC SCHMIDT DECOMPOSITION OF GAUSSIAN KERNEL

In the usual pump-degenerate schemes, i.e., SPDC or one-pump SFWM, the nonlinear interaction along the waveguide is constant. This entails that the phase-matching function, which is used in the spectral description of the joint signal-idler distribution [43,44], takes the form of a sinc-function which inevitably results in spectral correlations in the signal-idler photon pair. Note that the same spectral behavior results from performing a two-dimensional Fourier transform of the JTA in Eq. (20) due to the presence of the Heaviside functions [see also Fig. 2(a)]. Fortunately, this behavior may be avoided by the use of dual-pump SFWM if the pump-pump overlap is vanishing at the endpoints of the waveguide and optimal halfway through the waveguide. In addition to showing great promise with respect to generation of pure single-photon states, this case holds the advantage of enabling simple analytical expressions for both the purity and the pair-production rate [see Eqs. (27) and (28)].

In the case of a full symmetric pump-pump collision between Gaussian pulses, the JTA has the simple form

$$\mathcal{A}_t(t_s,t_r) = K\exp\left[-\frac{(t_c-\beta_p z_c+\beta_p l/2)^2}{2\tau_p}\right] \times \exp\left[-\frac{(t_c-\beta_q z_c+\beta_q l/2)^2}{2\tau_q}\right], \tag{B1}$$

in which we have neglected the effects of NPM and defined $K = i\gamma\varepsilon(E_pE_q/\pi\tau_p\tau_q)^{1/2}/\beta_{rs}$. The relative temporal delays of $\beta_{p,q}l/2$ ensure that the largest pump-pump overlap occurs halfway through the waveguide in agreement with Eq. (23). By inserting the collision coordinates from Eq. (21), the effect of the symmetric relative temporal delays become apparent as Eq. (B1) may be rewritten as

$$\mathcal{A}_t(t_s,t_r) = K\exp\left\{-\frac{[\beta_{rp}(t_s-\beta_s l/2)-\beta_{sp}(t_r-\beta_r l/2)]^2}{2\beta_{rs}^2\tau_p^2} - \frac{[\beta_{rq}(t_s-\beta_s l/2)-\beta_{sq}(t_r-\beta_r l/2)]^2}{2\beta_{rs}^2\tau_q^2}\right\}. \tag{B2}$$

It appears from Eqs. (B2) and (31) that the Schmidt modes v_{sj} are centered at $t_s = \beta_s l/2$ and the modes v_{rj} are centered

at $t_r = \beta_r l/2$. Making the substitutions $t_j - \beta_j l/2 \to t_j$ (this change has no influence on the pair-production rate or the purity of a heralded single-photon state), it is a simple task to put the JTA in the simple form

$$\mathcal{A}_t(t_s,t_r) = K \exp\left(- \frac{a t_s^2 - 2b t_s t_r + c t_r^2}{2} \right), \tag{B3}$$

where the three real coefficients obey $a > 0$, $c > 0$, and $ac - b^2 > 0$ and are given as

$$a = \alpha_{rp}^2 + \alpha_{rq}^2, \tag{B4}$$

$$b = \alpha_{rp}\alpha_{sp} + \alpha_{rq}\alpha_{sq}, \tag{B5}$$

$$c = \alpha_{sp}^2 + \alpha_{sq}^2, \tag{B6}$$

where $\alpha_{jk} = \beta_{jk}/(\beta_{rs}\tau_k)$. The mixed term in Eq. (B3), which accounts for temporal correlation between the signal and idler photons, disappears when $\alpha_{rp}\alpha_{sp} = -\alpha_{rq}\alpha_{sq}$. This purity criterion is equivalent to Eq. (29). Furthermore, the Gaussian kernel in Eq. (B3) has an analytical Schmidt decomposition (for a thorough derivation, see Appendix A of Ref. [26]), for which the two sets of Schmidt modes take the form of the normalized Hermite–Gaussian functions and the Schmidt coefficients satisfy

$$\lambda_n^2 = |K|^2 \pi (1-\kappa^2)\kappa^{2n}\tau_s\tau_r, \tag{B7}$$

where

$$\kappa = \frac{(ac)^{1/2} - (ac-b^2)^{1/2}}{b}, \tag{B8}$$

$$\tau_s = \left[\frac{c}{a(ac-b^2)} \right]^{1/4}, \tag{B9}$$

$$\tau_r = \left[\frac{a}{c(ac-b^2)} \right]^{1/4}. \tag{B10}$$

From Eqs. (B7)–(B10) one can find the purity $\mathcal{P}$ and the generation rate R in terms of the coefficients a, b, and c. They are given as

$$\mathcal{P}_{a,b,c} = [(ac-b^2)/(ac)]^{1/2}, \tag{B11}$$

and

$$R_{a,b,c} = |K|^2/(ac-b^2)^{1/2}. \tag{B12}$$

Finally, by insertion of Eqs. (B4)–(B6), one immediately recovers Eqs. (27) and (28), as required.

Finally, we show explicitly why the proposed scheme is inaccessible for single-pump configurations. To this end, instead of neglecting the Heaviside functions as in Eq. (B1), we approximate their product by an effective Gaussian [10,17,26]. For the shifted time variables defined below Eq. (B2), the Heaviside functions are approximated according to

$$\begin{aligned} &\mathrm{H}(t_s - t_r + \beta_{rs}l/2)\mathrm{H}(t_r - t_s + \beta_{rs}l/2) \\ &\quad \approx h \exp\left[- \frac{(t_s - t_r)^2}{2w(\beta_{rs}l/2)^2} \right], \end{aligned} \tag{B13}$$

where h and w are fitting parameters on the order of unity, which are otherwise unimportant. This approximation enables us to obtain the conditions under which boundary effects are negligible. To clarify, consider first the dual-pump configuration which allows a large purity if $\alpha_{rp}\alpha_{sp} + \alpha_{rq}\alpha_{sq} \approx 0$. In this case, the boundary effects are negligible if $\min\{a,c\} > (\beta_{rs}l/2)^{-2}$. In other words, the condition enabling a full pump-pump collision can be formulated as

$$\min\left\{ \frac{\beta_{rp}^2}{\tau_p^2} + \frac{\beta_{rq}^2}{\tau_q^2}, \frac{\beta_{sp}^2}{\tau_p^2} + \frac{\beta_{sq}^2}{\tau_q^2} \right\} > \frac{4}{l^2}. \tag{B14}$$

Conversely, for a single-pump configuration, the purity criterion is formulated as $-2\alpha_{rp}\alpha_{sp} = (\beta_{rs}l/2)^{-2}$ [10,17] and, in fact, this entails that boundary effects must play an important role. To illustrate, assume that $a = 2\alpha_{rp}^2 > (\beta_{rs}l/2)^{-2}$. Due to the above criterion for purity, this immediately leads to the opposite inequality for c; that is, $c = 2\alpha_{sp}^2 < (\beta_{rs}l/2)^{-2}$. Thus, to sum up, the condition $\min\{a,c\} > (\beta_{rs}l/2)^{-2}$ can never be obeyed for a single-pump configuration which, in agreement with intuition, means that boundary effects are always present.

APPENDIX C: REDUCED STATE AND HERALDING

To examine the process of heralding we must consider the density operator $\hat{\rho} = |\psi\rangle\langle\psi|$, where the quantum state $|\psi\rangle$ resulting from SFWM is given by Eq. (12). In the course of this analysis, we need to trace density operators of the general form

$$\begin{aligned} \hat{\rho} \;&=\; \iint dt_k dt_l M(t_k,t_l)\hat{a}^\dagger(t_k)\,|0\rangle\,\langle 0|\,a(t_l) \\ &\to \sum_{k,l}^{n} M_{kl}\hat{a}_k^\dagger\,|\{0\}\rangle\,\langle\{0\}|\,\hat{a}_l, \end{aligned} \tag{C1}$$

where $M(t_k,t_l)$ is an arbitrary function of its arguments. The second version of Eq. (C1) is the discrete version of the first with $|\{0\}\rangle = |0_1,\ldots,0_n\rangle$ being an n-dimensional vacuum state. For each temporal component i we have the partial trace

$$\mathrm{Tr}_i(\rho) = \langle 0_i|\hat{\rho}|0_i\rangle + \langle 1_i|\hat{\rho}|1_i\rangle\,, \tag{C2}$$

where $|0_i\rangle$ and $|1_i\rangle$ are the zero- and one-photon states for component i only (including photon states of higher photon numbers has no effect in this case). Combining Eqs. (C1) and (C2) yields

$$\mathrm{Tr}_i(\rho) = M_{ii}\,|\{0_i'\}\rangle\,\langle\{0_i'\}| + \sum_{k,l\neq i} M_{kl}\hat{a}_k^\dagger\,|\{0_i'\}\rangle\,\langle\{0_i'\}|\,\hat{a}_l, \tag{C3}$$

where $|\{0_i'\}\rangle = |0_1,\ldots,0_{i-1},0_{i+1},\ldots,0_n\rangle$ is an $(n-1)$-dimensional vacuum state. Note that the first term in Eq. (C3) stems from the inner product with $|1_i\rangle$ and the summation results from the inner product with $|0_i\rangle$. Sequentially performing this operation over all n discrete components yields the complete trace

$$\mathrm{Tr}(\hat{\rho}) = \sum_i M_{ii} \to \int dt_i M(t_i,t_i), \tag{C4}$$

where the second version is now the continuous version of the first.

Returning to the density operator $\hat{\rho}$ associated with the state generated from SFWM, it may be written as

$$\hat{\rho} = |\psi_0\rangle\,\langle\psi_0| + |\psi_1\rangle\,\langle\psi_0| + |\psi_0\rangle\,\langle\psi_1| + |\psi_1\rangle\,\langle\psi_1|\,, \tag{C5}$$

where $|\psi_0\rangle$ and $|\psi_1\rangle$ correspond to the two terms in Eq. (12) (which were derived in Appendix A). To obtain the reduced density operator for the signal, one can sequentially trace the idler degrees of freedom for the four terms in Eq. (C5). Using the discretization method outlined above, it is a simple exercise to show that

$$\mathrm{Tr}_r(|\psi_0\rangle\langle\psi_0|) = |0\rangle\langle 0|\,, \tag{C6}$$

and

$$\mathrm{Tr}_r(|\psi_0\rangle\langle\psi_1|) = \mathrm{Tr}_r(|\psi_1\rangle\langle\psi_0|) = 0. \tag{C7}$$

To evaluate the partial trace of the last term in Eq. (C5) we invoke the result from Eqs. (C1)–(C4) while noting that the idler part of Eq. (A12) is similar to Eq. (C1). We find that

$$\mathrm{Tr}_r(|\psi_1\rangle\langle\psi_1|) = \iint dt_s' dt_s'' \mathcal{K}_s(t_s',t_s'')\hat{a}_s^\dagger(t_s')\,|0\rangle\langle 0|\,\hat{a}_s(t_s''), \tag{C8}$$

where the signal kernel

$$\mathcal{K}_s(t_s',t_s'') = \int dt_r \mathcal{A}_t(t_s',t_r)\mathcal{A}_t^*(t_s'',t_r) \tag{C9}$$

is Hermitian, $\mathcal{K}_s(t_s',t_s'') = \mathcal{K}_s^*(t_s'',t_s')$. Combining the preceding results, the reduced state of the signal has the density operator

$$\hat{\rho}_s = |0\rangle\langle 0| + \iint dt_s' dt_s'' \mathcal{K}_s(t_s',t_s'')\hat{a}_s^\dagger(t_s')\,|0\rangle\langle 0|\,\hat{a}_s(t_s''), \tag{C10}$$

which evidently does *not* describe the process of heralding in which signal information is retained only if an idler photon is detected. Instead, let $\hat{n}_r$ be the idler number operator. Then a heralded signal photon is described by the reduced density operator

$$\begin{aligned}\hat{\rho}_{sh} &= \mathrm{Tr}_r(|\psi\rangle\langle\psi|\,\hat{n}_r) = \mathrm{Tr}_r[(|\psi_0\rangle + |\psi_1\rangle)\langle\psi_1|\,\hat{n}_r] \\ &= \mathrm{Tr}_r[(|\psi_0\rangle + |\psi_1\rangle)\langle\psi_1|] = \mathrm{Tr}_r(|\psi_1\rangle\langle\psi_1|).\end{aligned} \tag{C11}$$

Thus, the density operator for a heralded signal is simply the partial idler trace of the biphoton part of the output quantum state given by Eq. (C8). Note that the heralded signal state is also uniquely determined by the JTA through the signal kernel in Eq. (C9), which appears twice in the expression for the purity in Eq. (25). Expressing the signal kernel in terms of the JTA Schmidt decomposition in Eq. (31), yields

$$\mathcal{K}_s(t_s',t_s'') = \sum_j \lambda_j^2 v_{sj}(t_s')v_{sj}^*(t_s''). \tag{C12}$$

The heralded signal photon is in general in a mixed state of temporal wave-packet modes v_{sj} with weights λ_j^2. Only if $\lambda_j = 0$ for $j > 1$ is the photon in a truly pure state, as required for optimal quantum interference.

[1] N. Gisin and R. Thew, Nat. Photonics **1**, 165 (2007).
[2] N. Gisin, G. Ribordy, W. Tittel, and H. Zbinden, Rev. Mod. Phys. **74**, 145 (2002).
[3] E. Knill, R. Laflamme, and G. J. Milburn, Nature (London) **409**, 46 (2001).
[4] C. Gerry and P. Knight, *Introductory Quantum Optics* (Cambridge University Press, Cambridge, 2005).
[5] M. Eisaman, J. Fan, A. Migdall, and S. Polyakov, Rev. Sci. Instrum. **82**, 071101 (2011).
[6] D. C. Burnham and D. L. Weinberg, Phys. Rev. Lett. **25**, 84 (1970).
[7] J. Chen, X. Li, and P. Kumar, Phys. Rev. A **72**, 033801 (2005).
[8] C. K. Hong, Z. Y. Ou, and L. Mandel, Phys. Rev. Lett. **59**, 2044 (1987).
[9] I. A. Walmsley and M. G. Raymer, Science **307**, 1733 (2005).
[10] P. J. Mosley, J. S. Lundeen, B. J. Smith, and I. A. Walmsley, New J. Phys. **10**, 093011 (2008).
[11] P. J. Mosley, J. S. Lundeen, B. J. Smith, P. Wasylczyk, A. B. U'Ren, C. Silberhorn, and I. A. Walmsley, Phys. Rev. Lett. **100**, 133601 (2008).
[12] J. L. O'Brien, G. J. Pryde, A. G. White, T. C. Ralph, and D. Branning, Nature (London) **426**, 264 (2003).
[13] C. Söller, O. Cohen, B. J. Smith, I. A. Walmsley, and C. Silberhorn, Phys. Rev. A **83**, 031806 (2011).
[14] Y.-P. Huang and P. Kumar, Phys. Rev. A **84**, 032315 (2011).
[15] D. V. Reddy, M. G. Raymer, and C. J. McKinstrie, Phys. Rev. A **91**, 012323 (2015).
[16] J. B. Christensen, D. V. Reddy, C. J. McKinstrie, K. Rottwitt, and M. G. Raymer, Opt. Express **23**, 23287 (2015).
[17] W. P. Grice, A. B. U'Ren, and I. A. Walmsley, Phys. Rev. A **64**, 063815 (2001).
[18] A. B. U'Ren, C. Silberhorn, R. Erdmann, K. Banaszek, W. P. Grice, I. A. Walmsley, and M. G. Raymer, Laser Phys. **15**, 146 (2005).
[19] K. Garay-Palmett, H. J. McGuinness, O. Cohen, J. S. Lundeen, R. Rangel-Rojo, A. B. U'Ren, M. G. Raymer, C. J. McKinstrie, S. Radic, and I. A. Walmsley, Opt. Express **15**, 14870 (2007).
[20] O. Cohen, J. S. Lundeen, B. J. Smith, G. Puentes, P. J. Mosley, and I. A. Walmsley, Phys. Rev. Lett. **102**, 123603 (2009).
[21] M. Halder, J. Fulconis, B. Cemlyn, A. Clark, C. Xiong, W. J. Wadsworth, and J. G. Rarity, Opt. Express **17**, 4670 (2009).
[22] B. J. Smith, P. Mahou, O. Cohen, J. S. Lundeen, and I. A. Walmsley, Opt. Express **17**, 23589 (2009).
[23] L. E. Vicent, A. B. U'Ren, R. Rangarajan, C. I. Osorio, J. P. Torres, L. Zhang, and I. A. Walmsley, New J. Phys. **12**, 093027 (2010).
[24] C. J. McKinstrie, S. Radic, and A. R. Chraplyvy, IEEE J. Sel. Top. Quantum Electron. **8**, 538 (2002); **8**, 956 (2002)(E).
[25] C. J. McKinstrie, M. Yu, M. G. Raymer, and S. Radic, Opt. Express **13**, 4986 (2005).
[26] L. Mejling, C. J. McKinstrie, M. G. Raymer, and K. Rottwitt, Opt. Express **20**, 8367 (2012).
[27] B. Fang, O. Cohen, J. B. Moreno, and V. O. Lorenz, Opt. Express **21**, 2707 (2013).

[28] A. M. Brańczyk, A. Fedrizzi, T. M. Stace, T. C. Ralph, and A. G. White, Opt. Express **19**, 55 (2011).
[29] J. Fan and A. Migdall, Opt. Express **13**, 5777 (2005).
[30] C. Reimer, M. Kues, L. Caspani, B. Wetzel, P. Roztocki, M. Clerici, Y. Jestin, M. Ferrera, M. Peccianti, A. Pasquazi *et al.*, Nat. Commun. **6**, 8236 (2015).
[31] B. Bell, A. McMillan, W. McCutcheon, and J. Rarity, Phys. Rev. A **92**, 053849 (2015).
[32] Q. Lin, F. Yaman, and G. P. Agrawal, Phys. Rev. A **75**, 023803 (2007).
[33] G. P. Agrawal, *Nonlinear Fiber Optics* (Elsevier, Amsterdam, 2013).
[34] R. W. Boyd, *Nonlinear Optics* (Academic Press, New York, 2008).
[35] L. Mejling, D. S. Cargill, C. J. McKinstrie, K. Rottwitt, and R. O. Moore, Opt. Express **20**, 27454 (2012).
[36] C. J. McKinstrie, Opt. Commun. **282**, 583 (2009).
[37] S. L. Braunstein, Phys. Rev. A **71**, 055801 (2005).
[38] C. J. McKinstrie and M. Karlsson, Opt. Express **21**, 1374 (2013).
[39] H. J. McGuinness, M. G. Raymer, and C. J. McKinstrie, Opt. Express **19**, 17876 (2011).
[40] D. V. Reddy, M. G. Raymer, C. J. McKinstrie, L. Mejling, and K. Rottwitt, Opt. Express **21**, 13840 (2013).
[41] D. L. P. Vitullo and M. G. Raymer (private communication).
[42] C. J. McKinstrie, M. G. Raymer, S. Radic, and M. V. Vasilyev, Opt. Commun. **257**, 146 (2006).
[43] T. E. Keller and M. H. Rubin, Phys. Rev. A **56**, 1534 (1997).
[44] W. P. Grice and I. A. Walmsley, Phys. Rev. A **56**, 1627 (1997).